A Simultaneous Wireless Power and Data Transfer Method Utilizing a Novel Coupler Design for Rotary Steerable Systems

Xiaofei Li, *Member, IEEE*, Zhiheng Li, *Graduate Student Member, IEEE*, Udaya K. Madawala, *Fellow, IEEE*, Heshou Wang, Yue Sun, *Member, IEEE*, Xin Dai, *Member, IEEE*, and Jiefeng Hu, *Senior Member, IEEE*

***Abstract*—This article introduces a simultaneous wireless power and data transfer method by using a half-cylinder-stator and quarter-cylinder-rotator coupling mechanism for rotary steerable systems. Through this configuration, stability and synchronization of both power and data transfers are ensured, notably under comprehensive 360° rotational conditions. Moreover, based on the decoupling characteristics, the interference between power and data transfer is also greatly reduced. A prototype is built, which illustrates that the proposed structure possesses the constant voltage output and stable data transfer capability. Furthermore, observations indicate that the output voltage can be maintained as stable at 48 V with a deviation of ±2.7%. And there is no detectable significant change in data transfer voltage amplitude. During the full 360° rotation, the system dc–dc efficiency range is from 86.7% to 88.9%.**

***Index Terms*—Magnetic coupling structure, rotary steerable systems (RSSs), simultaneous power and data transfer, wireless power transfer (WPT).**

I. Introduction

ROTARY steerable system (RSS) is acknowledged within the drilling industry as a fundamental instrument for horizontal and extended-reach wells [1]. These systems enable continuous adjustments to the drilling direction without the need to stop the drill's rotation, offering significant improvements in drilling efficiency and the ability to navigate complex geological formations. Unlike traditional directional drilling technology, the RSS allows the drill bit to penetrate high-quality reservoir sections along a predefined trajectory [2]. It substantially diminishes nonproductive time, dramatically accelerating the drilling pace, thereby enhancing oil and gas recovery and well production [3]. For the RSS, the demand for power transfer and real-time data transfer has become essential [4]. A key challenge in these applications is maintaining reliable power supply and real-time data communication under the harsh conditions of deep-earth drilling. In terms of supplying power to the electrical equipment of the RSS, one method is to use a battery to power it [5]. However, the battery-driven approach is hindered by challenges, including finite lifespan and the laboriousness of replacements [6]. Another method for supplying power to the electrical equipment of the RSS is through a contact slip ring, which transfers power between the stator side and the rotator side. However, the susceptibility of contact slip rings to abrasion often results in inefficiencies and safety concerns [7]. To solve the problem of contact slip rings, researchers have proposed noncontact slip rings based on wireless power transfer (WPT) technology [8], [9]. By eliminating the need for physical contact, WPT addresses both wear and power issues, improving longevity, reliability, and a safer operational environment [10], [11].

In the context of RSSs, it is essential to acknowledge that their importance transcends mere power transfer, encompassing also the critical aspect of data transfer [12]. It is acknowledged that these conventional modules (e.g., Wi-Fi, ZigBee, etc.), although prevalent, require processes such as pairing and are often subject to transfer delays [13], [14]. Hence, recent investigations gradually demonstrated that data can be transmitted via the existing power transfer channels. This method of simultaneous wireless power and data transfer (SWPDT) presents a more straightforward alternative [15]. There are two primary methodologies for SWPDT [16]: 1) the shared channel type, which means transmitting power and data through the same coupling mechanism; 2) the separate channel type, which means transmitting power and data through a separate coupling mechanism.

As for the shared channel type, based on different modulation methods, it can be further divided into energy modulation type [17], [18], and carrier modulation type [19]. Specifically, Son

Manuscript received 29 February 2024; revised 30 April 2024 and 27 May 2024; accepted 31 May 2024. Date of publication 4 June 2024; date of current version 16 July 2024. This work was supported by the National Natural Science Foundation of China under Grant 52007012. Recommended for publication by Associate Editor A. Kuperman. *(Corresponding authors: Xiaofei Li; Heshou Wang.)*

Xiaofei Li, Zhiheng Li, Yue Sun, and Xin Dai are with the School of Automation, Chongqing University, Chongqing 400044, China (e-mail: xiaofei.li@cqu.edu.cn; zhihengli@ieee.org; syue06@cqu.edu.cn; toybear@vip.sina.com).

Udaya K. Madawala is with the Department of Electrical and Computer Engineering, The University of Auckland, Auckland 1010, New Zealand (e-mail: u.madawala@auckland.ac.nz).

Heshou Wang is with the Department of Electrical Engineering, The Hong Kong Polytechnic University, Hung Hom, Hong Kong (e-mail: hs.wang@polyu.edu.hk).

Jiefeng Hu is with the Institute of Innovation, Science and Sustainability, Federation University Australia, Mount Helen, VIC 3353, Australia, and also with the Centre for New Energy Transition Research, Federation University Australia, Mount Helen, VIC 3353, Australia (e-mail: j.hu@federation.edu.au).

Color versions of one or more figures in this article are available at https://doi.org/10.1109/TPEL.2024.3409358.

Digital Object Identifier 10.1109/TPEL.2024.3409358

and Jang [17] propose a data transfer technique founded on the concept of energy injection, wherein data modulation is achieved by varying the voltage at the transmitter side. Subsequently, demodulation is executed by harnessing the attributes of the energy flow. Nevertheless, this data transfer method may be affected by power voltage disturbances, and the output voltage of power transfer would deteriorate. Yue et al. [18] detail an approach where the data intended for transfer is utilized as a switching signal. This methodology involves altering the resonant capacitance at the receiving end at the point of zero voltage crossing, consequently modifying the reflective impedance. This adjustment impacts the current amplitude in the transmitting end's loop. The demodulation of the data is ultimately achieved by the demodulation circuit, which bases its operation on the current amplitude present at the power transmitting end. In summary, it is evident that the energy modulation type accomplishes data transfer by establishing a correlation between the "power waveform" and the binary 0/1 signal. This is achieved through modifications in the amplitude of the power waveform, thereby enabling the effective conveyance of the signal.

In terms of the carrier modulation, some scholars employ a sine wave carrier as the modulation waveform, utilizing a time-division multiplexing approach for the transfer of power and signals over the same pair of coupling coils, but in distinct time periods [20]. Notably, the duration allocated for data transfer is shorter compared to that for power transfer. Consequently, this method minimally affects power transfer. However, it is observed that as the system's power level escalates, the complexity associated with data demodulation proportionally increases. As for petroleum drilling systems, Jia et al. [4] propose a SWPDT method based on carrier modulation. The interference between power and data transfer is relatively large. The interference was filtered out by using the wave trappers. However, to attain optimal filtering efficacy, a complicated design of these wave trappers is needed as they should resonate accurately.

For the separate channel type, Wang et al. [21] propose a SWPDT method where power and data are transferred through separate coupling coils. The results show that the interference between power and data transfer is relatively small, and it can be further minimized by intentionally increasing the distance between power and data coupling mechanisms. As a result, while this method can simplify the design of data processing circuits, the increased distance between the power and data channels enlarges the dimensions of the entire system. Such an increase in size renders this design less suitable for rotary drilling systems, which typically have stringent volume and size constraints.

Hence, this article investigates a separated channel SWPDT system with a half-cylinder-stator and quarter-cylinder-rotator coupling mechanism for RSSs, ensuring stable power and data transfer even during 360° rotation. The system minimizes interference between power and data transfer, providing constant voltage (CV) and stable data regardless of rotational alignment or load changes. In addition, its design allows close placement of power and data coils due to negligible cross-mutual inductance, resulting in a compact and efficient design for rotary steerable systems.

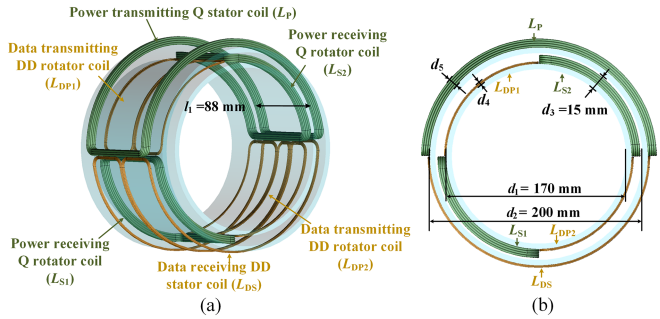

Fig. 1. Magnetic coupling structure. (a) Overview. (b) Top view with detailed size information.

TABLE I
SPECIFIC PARAMETERS OF THE DESIGNED COUPLER

Description	Symbol	Value
External diameter of inner cylinder	d_1	170 mm
External diameter of outer cylinder	d_2	200 mm
Gap between two cylinders	d_3	15 mm
Thickness of DD coil	d_4	1 mm
Thickness of Q coil	d_5	6 mm
Height of the magnetic coupler	l_1	88 mm
Material of Q and DD coils	/	Copper litz wire
Material of cylindrical skeleton	/	Acrylic

II. ROTARY COUPLING MECHANISMS

A. System Overview

The proposed coupler comprises two distinct cylinders: an outer stationary cylinder (stator) and an inner rotary cylinder (rotator), as illustrated in Fig. 1(a). The Q coil is designed with three layers, and each layer holds three turns of a 2-mm wire diameter. In contrast, the DD coil is designed with one layer for data transfer, and each layer comprises three turns of 1-mm wire diameter. It is worth noting that this design allows for flexibility in the number of layers of Q and DD coils. The selection of Q and DD coil structures is driven by their unique characteristics, as they can be decoupled from each other [8]. The number of strands of the litz wire for the Q coil and DD coil are 250 and 50, respectively.

Then, Fig. 1(b) shows the dimension information from the top view, and the detailed size information about d_1, d_2, d_3, d_4, d_5, and l_1 is shown in Table I. The material of the coils is copper litz wire whereas the material of the cylindrical skeleton is acrylic.

B. Half-Cylinder Stator

The stator keeps stationary with the drilling pipe, consisting of the power transmitting part and data receiving part that can collect the information from the rotator side. As illustrated in Fig. 2(a), the stator integrates two main coil types: one Q coil (i.e., L_{P}) and one DD oil (i.e., L_{DS}). Spanning 180° each, the Q is designed for power transmitting function whereas the DD coil specializes in data receiving function.

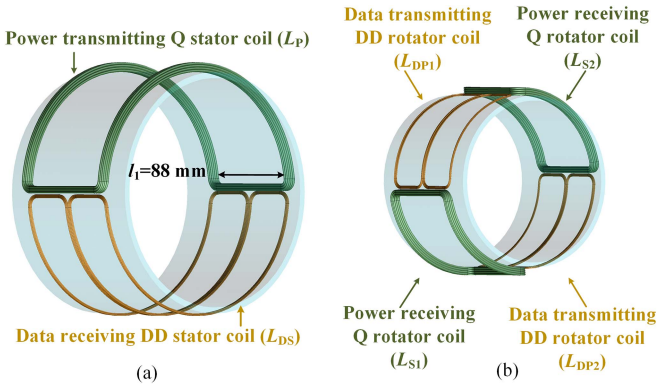

Fig. 2. (a) Half-cylinder stator. (b) Quarter-cylinder rotator.

C. Quarter-Cylinder Rotator

The rotator, equipped with a data transmitting and power receiving part, rotates all around 360° along with the rotary steerable part. As shown in Fig. 2(b), such a configuration is the diagonal placement of the coils; namely, coils situated on diagonals are homogeneous in type, being either Q or DD. Two Q coils (i.e., L_{S1} and L_{S2}) are designed for power receiving, whereas two DD coils (i.e., L_{DP1} and L_{DP2}) are aimed at data transmitting.

D. Mutual Inductance Versus Rotatory Misalignment

As for the data transfer, M_{DD1} denotes the mutual inductance between L_{DP1} and L_{DS}, while M_{DD2} characterizes the mutual inductance between L_{DP2} and L_{DS}. During the rotational operation from 0 to 90° (180° to 270°) shown in Fig. 3(a), there is an observed increment (decrement) in M_{DD1}, whilst M_{DD2} exhibits a concomitant decrement (increment). Therefore, L_{DP1} and L_{DP2} are connected in series in this article to form the data transmitting coil L_{DP} (i.e., $L_{DP} = L_{DP1}+L_{DP2}$), and their cumulative effect is M_{DD} (i.e., $M_{DD} = M_{DD1}+M_{DD2}$) keeps relatively stable due to the proposed half-cylinder stator and quarter-cylinder rotator coupling mechanism. The measured range for M_{DD} is from 5.86 to 6.05 μH. When contrasted with its mean value of 5.94 μH, it exhibits a fluctuation within $\pm$1.85%. Such stability infers a consistent data transfer capability.

With respect to the power transfer, M_{PP1} represents the mutual inductance between L_{S1} and L_P, whereas M_{PP2} denotes the mutual inductance of L_{S2} and L_P. During the rotational operation from 90° to 180° (270° to 360°) shown in Fig. 3(b), there is an observed increment (decrement) in M_{PP1}, whereas M_{PP2} exhibits a concomitant decrement (increment). Similarly, two Q coils are also connected in series (i.e., $L_S = L_{S1}+L_{S2}$) for receiving power. The mutual inductance between L_S and L_P is M_{PP} (i.e., $M_{PP} = M_{PP1}+M_{PP2}$). As can be seen from the measured results, M_{PP} remains relatively stable due to the proposed half-cylinder stator and quarter-cylinder rotator coupling mechanism. The value spans between 18.55 and 19.48 μH. When compared to its mean value of 19.02 μH, the data fluctuates within a range of approximately $\pm$2.42%.

As shown in Fig. 3(c), $M_{LDP\text{-}LP}$, $M_{LDP\text{-}LS}$, $M_{LDS\text{-}LP}$, and $M_{LDS\text{-}LP}$ are unwanted cross-coupled mutual inductances

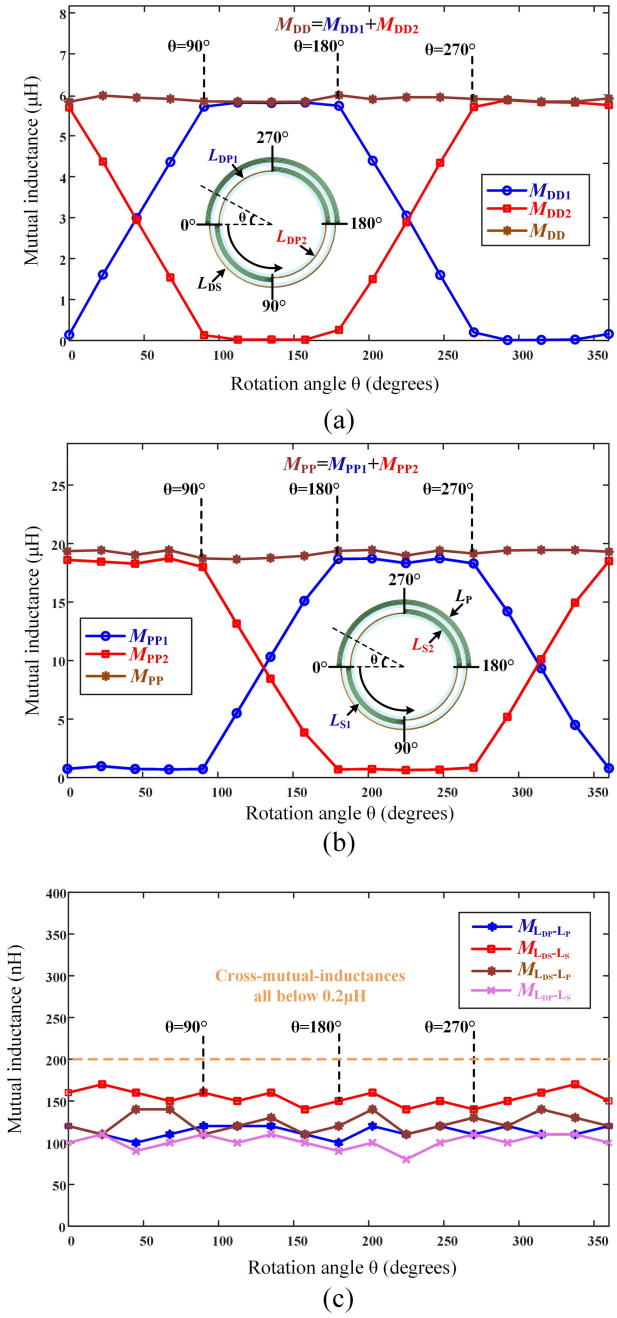

Fig. 3. Variation of the mutual inductance in the presented WPT system in (a) data transfer, (b) power transfer, and (c) the cross-coupled mutual inductances.

among coils L_{DP}, L_{DS}, L_P, and L_S. Thanks to the decoupling characteristics between DD and Q coils [22], all these measured values consistently remain below 0.2 μH. These small enough values indicate that the interference between power transfer and data transfer is small enough to be negligible [23]. Moreover, the maximum speed of the rotator in the RSS is about 400 revolutions per minute [24]. Due to the proposed half-cylinder-stator and quarter-cylinder-rotator coupling mechanism, the equivalent mutual inductance remains consistently stable under all 360° rotary conditions. As a result, the performance of the system

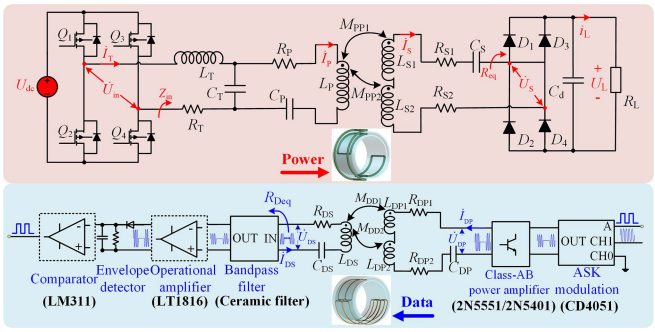

Fig. 4. Circuitry diagram of the presented WPT system with the power and data channels.

remains unaffected by variations in the rotational speed of the rotator [25].

III. Circuit Topology Analysis

Fig. 4 depicts the circuit diagram of the presented WPT system, where the inductor-capacitor-capacitor-series (*LCC*-S) compensation topology is utilized in power transfer, which can provide a CV output independent of load changes. As for data transfer, to enhance its transfer capability, a relatively simple series-series (S-S) compensation topology is utilized [26].

A. Analysis of Power Transfer

The inverter architecture is constituted by MOSFETs (Q_1–Q_4), whereas the rectifier is made up of diodes (D_1–D_4). R_{eq} symbolizes the equivalent input resistance of the rectifier. The load resistance is R_L. There is no control over the power supply and the system operates in an open loop. Given the usage of the fundamental harmonics approximation, the output voltage of the inverter can be expressed in its phasor form as [27]

$$\dot{U}_{in} = \frac{2\sqrt{2}U_{dc}}{\pi}\angle 0^\circ \tag{1}$$

where the output voltage of the inverter can be regarded as constant.

According to Kirchhoff's voltage law (KVL), the following equations can be gained:

$$\begin{cases} \dot{U}_{in} = (j\omega L_T + R_T)\dot{I}_T + \frac{1}{j\omega C_T}(\dot{I}_T - \dot{I}_P) \\ \frac{1}{j\omega C_T}(\dot{I}_T - \dot{I}_P) = (R_P + j\omega L_P + \frac{1}{j\omega C_P})\dot{I}_P - j\omega M_{PP}\dot{I}_S \\ j\omega M_{PP}\dot{I}_P = (R_{S1} + R_{S2} + j\omega L_S + \frac{1}{j\omega C_S})\dot{I}_S + \dot{U}_S \\ \dot{U}_S = \frac{2\sqrt{2}}{\pi}U_L = \dot{I}_S R_{eq}, U_L = I_L R_L, R_{eq} = \frac{8}{\pi^2}R_L \end{cases} \tag{2}$$

where R_P (0.19 Ω), R_T (0.05 Ω), R_{S1} (0.11 Ω), and R_{S2} (0.11 Ω) are the corresponding inner resistances of L_P, L_T, L_{S1}, and L_{S2}, respectively. R_{S1} and R_{S2} can be regarded as a whole R_S (i.e., $R_S = R_{S1}+R_{S2}$). The relationship between inductors and capacitors can be simplified as

$$\omega L_T = \frac{1}{\omega C_T}, \omega L_P - \omega L_T = \frac{1}{\omega C_P}, \omega L_{S1} + \omega L_{S2} = \omega L_S = \frac{1}{\omega C_S}. \tag{3}$$

Substituting (3) and (1) into (2), U_L can be obtained as

$$U_L = \frac{\omega^2 M_{PP} U_{dc} C_T R_{eq}}{{C_T}^2 {M_{PP}}^2 R_T \omega^4 + {C_T}^2 R_P R_T \omega^2 (R_{eq} + R_S) + R_{eq} + R_S} \tag{4}$$

where ω is the operating angular frequency of power transfer, satisfying $\omega = 2\pi f, f = 85$ kHz [1]. Subsequently, the efficiency can be calculated as

$$\eta = \frac{\omega^4 {M_{PP}}^2 {L_T}^2 R_{eq}}{\left({M_{PP}}^2\omega^2 + R_P R_{eq} + R_P R_S\right)} \times \frac{1}{\left[{L_T}^2 (R_{eq} + R_S)\omega^2 + M_{PP} R_T \omega^2 + R_P R_T (R_{eq} + R_S)\right]}. \tag{5}$$

Then, the output impedance of the inverter can be calculated as

$$Z_{in} = \frac{\dot{U}_{in}}{\dot{I}_T} = \frac{(R_{eq} + R_S)\left(2R_T R_P + \omega^2 {L_T}^2\right) + R_T \omega^2 {M_{PP}}^2}{\left(2R_P R_{eq} + 2R_S R_P + \omega^2 {M_{PP}}^2\right)}. \tag{6}$$

From the analysis of (6), it is evident that when the load resistance (R_L) exhibits a purely resistive nature, the output impedance (Z_{in}) likewise assumes a purely resistive characteristic.

Concerning power transfer, R_T, R_P, and R_S are so tiny that they can be neglected for simplifying analysis [28]. Therefore, the output voltage can be simplified as

$$U_L = \frac{(M_{PP1} + M_{PP2})U_{dc}}{L_T} = \frac{M_{PP} U_{dc}}{L_T}. \tag{7}$$

As can be seen from (7), U_L is a load-independent output. And U_L is stable as long as M_{PP} can be maintained as relatively consistent.

Similarly, the output impedance of the inverter can be further simplified as

$$Z_{in} = \frac{\dot{U}_{in}}{\dot{I}_T} = \frac{{L_T}^2}{{M_{PP}}^2} R_{eq}. \tag{8}$$

B. Analysis of Data Transfer

In the present study, the method of amplitude shift keying (ASK) modulation is employed for the generation of data carriers. This can be described as follows:

$$s_{ASK}(t) = \begin{cases} A_H \cos(\omega_D t)\text{bit0} \\ A_L \cos(\omega_D t)\text{bit1} \end{cases} \tag{9}$$

where ω_D is the angular operating frequency of the data transfer, satisfying $\omega_D = 2\pi f_D$, $f_D = 1.5$ MHz. This frequency was chosen because the data transfer frequency should be chosen to be at least one order of magnitude higher than the power transfer frequency [21]. A_H, and A_L are the highest and lowest amplitudes of the carrier wave, respectively.

For the purpose of ensuring robust data transfer, a specially designed data transfer circuit has been implemented, as depicted in Fig. 4. Specifically, the CD4051 chip is utilized for the

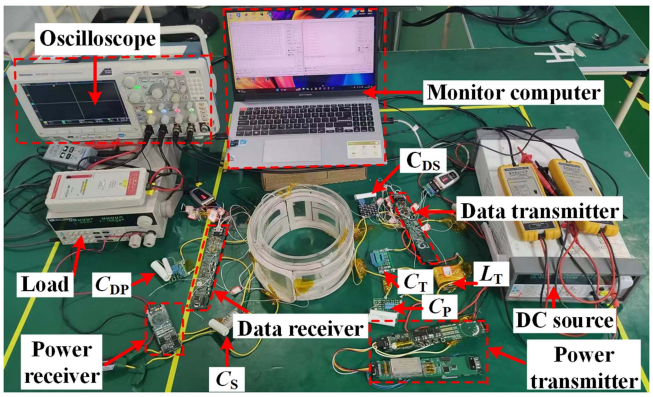

Fig. 5. Picture of the experimental setup.

application of ASK modulation. Power amplification within the system is achieved via a Class-AB configuration, employing the 2N5551 and 2N5401 transistors. Furthermore, the operational amplifier (OA) of the system is based on the LT1816 chip, while the comparator function is facilitated through the use of the LM311 chip. Then, the following equations can be established based on KVL:

$$\begin{cases} \dot{U}_{DP} = \\ \left(\frac{1}{j\omega_D C_{DP}} + j\omega_D L_{DP1} + j\omega_D L_{DP2} + R_{DP1} + R_{DP2}\right)\dot{I}_{DP} \\ \quad - j\omega_D M_{DD}\dot{I}_{DS} \\ 0 = \left(j\omega_D L_{DS} + \frac{1}{j\omega_D C_{DS}} + R_{DS}\right)\dot{I}_{DS} + \dot{U}_{DS} - j\omega_D M_{DD}\dot{I}_{DP} \\ \dot{U}_{DS} = \dot{I}_{DS} R_{Deq} \end{cases} \tag{10}$$

where inductors, capacitors, and resistors in the data transfer circuit should follow:

$$\omega_D(L_{DP1} + L_{DP2}) = \frac{1}{\omega_D C_{DP}}, \omega_D L_{DS} = \frac{1}{\omega_D C_{DS}}, R_{DP} = R_{DP1} + R_{DP2} \tag{11}$$

where R_{DP1}, R_{DP2}, and R_{DS} are the inner resistances of L_{DP1}, L_{DP2}, and L_{DS}, respectively.

Substituting (11) into (10) as well as ignoring the inner resistances, the root mean square value of $\dot{U}_{DS}$ can be expressed as

$$\left|\dot{U}_{DS}\right| = \frac{\left|\dot{U}_{DP}\right| R_{Deq}}{\omega_D(M_{DD1} + M_{DD2})} = \frac{\left|\dot{U}_{DP}\right| R_{Deq}}{\omega_D M_{DD}} \tag{12}$$

where R_{Deq} is the equivalent resistance seen from the bandpass filter. As can be seen in (12), the voltage amplitude for data transfer is stable as long as M_{DD} can be maintained as relatively constant.

IV. Experimental Verification

A laboratory setup is constructed to validate the proposed system, as depicted in Fig. 5. The utilized oscilloscope is MDO3024 from Tektronix, and the load is electronic load IT8512. The utilized dc power supply is SS-L605SPV from LCSC Electronics, and the MOSFET used in this study is IPB044N15N5 from

TABLE II
System Parameters

L_P	L_T	C_T	C_P	C_S	C_{DS}
84.2 μH	20 μH	175.3 nF	57 nF	32.6 nF	245 pF
C_{DP}	L_{DS}	L_{DP1}	L_{DP2}	L_{S1}	L_{S2}
274 pF	45.7 μH	20.4 μH	20.4 μH	53.8 μH	53.8 μH

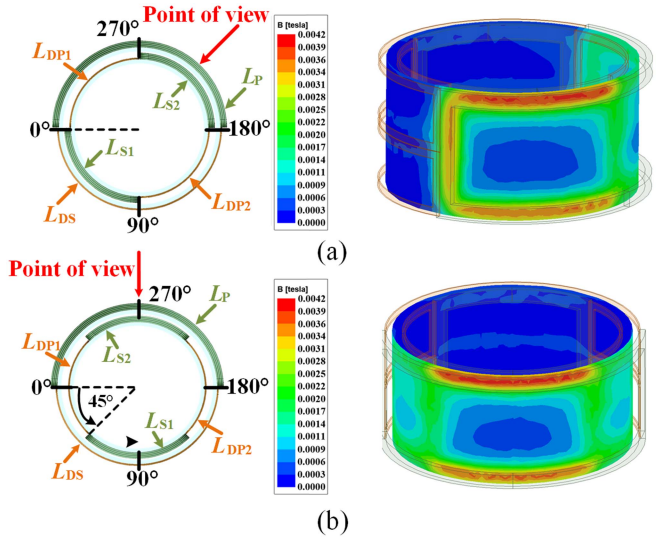

Fig. 6. Simulated magnetic field distribution. (a) From 225° point of view. (b) From 270° point of view.

Infineon. The detailed measured values can be seen in Table II. The input dc voltage of the system (U_{dc}) is 60 V. The output dc voltage (U_L) is set as 48 V, which is suitable for power drive orbit RSS from Schlumberger. The data transfer circuit and power transfer circuit are isolated from each other, and the transmitted data is sent by the monitoring computer.

Fig. 6 illustrates the magnetic field distribution viewed from two different points of view (i.e., 225° and 270°) to visualize the operating state of the coupler. These simulations are conducted under the operational conditions where the output voltage is 48 V, the load resistance is 10 Ω and the data transfer is in service. It can be seen in Fig. 6 that the magnetic field distribution between the coupled power transfer coils (i.e., L_P and L_{S2}) is relatively strong.

Fig. 7 illustrates the crucial waveforms of the inverter, namely the output voltage u_{in} and output current i_T. In order to accomplish zero-voltage switching (ZVS), the resonant capacitors can be strategically designed with a slightly smaller value than that derived from (3) [29]. By doing this, Z_{in} can exhibit an inductive characteristic. Accordingly, this can be exhibited by the fact that i_T slightly lags behind u_{in}, which validates the capability of achieving ZVS.

Fig. 8 shows the key waveforms of the data transfer circuit from data input to data output, where Fig. 8(a) shows the waveforms of the data transmitting side, whereas Fig. 8(b) shows the waveforms of the data receiving side. As can be seen in Fig. 8(a), the waveforms of u_{DP}, the modulation signal, the data carrier, and the input data are shown in oscilloscope channels #1, #2, #3, and #4, respectively. Fig. 8(b) shows that the waveforms of u_{DS},

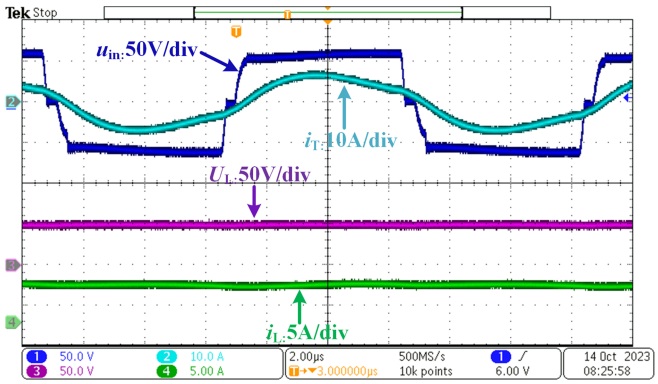

Fig. 7. Experimental validation of zero voltage switching.

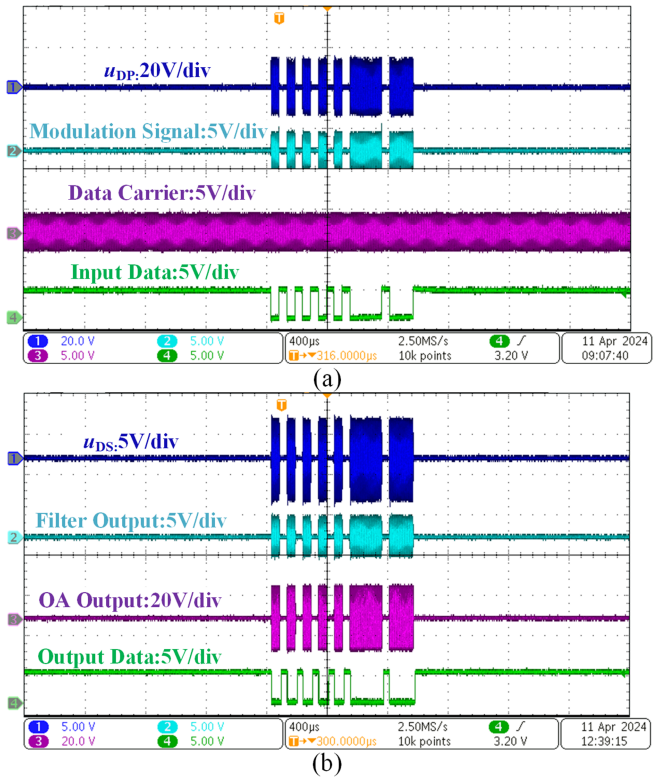

Fig. 8. Key waveforms of the data transfer circuit. (a) Data transmitting side. (b) Data receiving side.

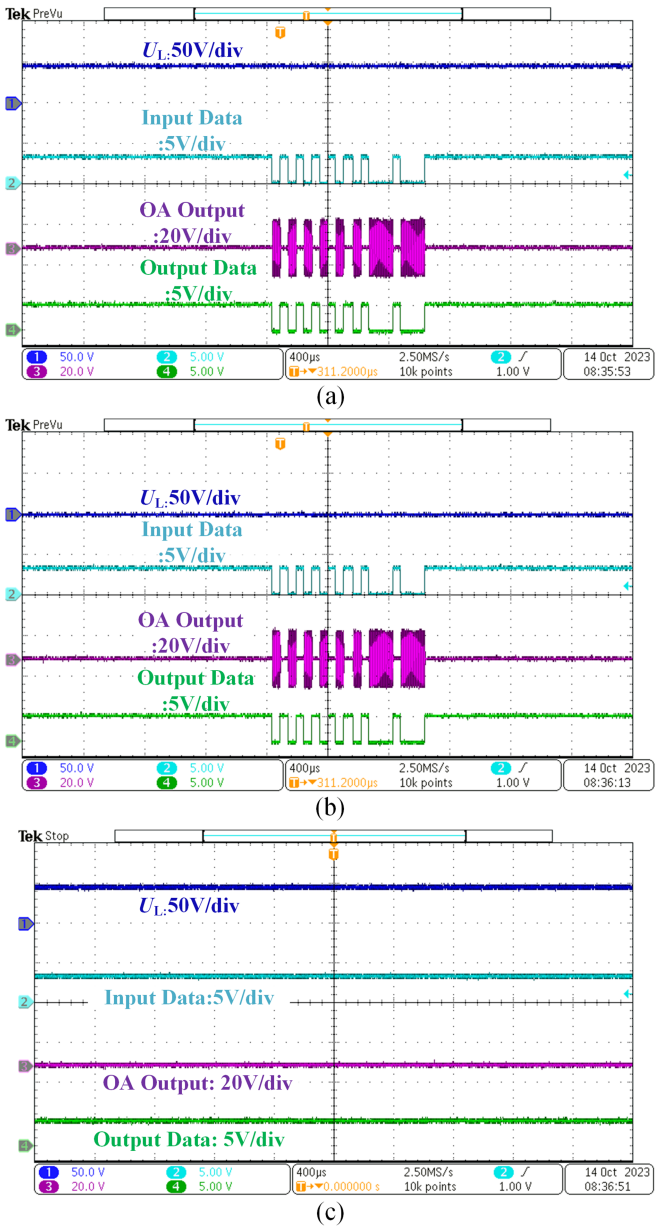

Fig. 9. Waveforms of synchronous parallel transfer of power and data in three operating modes. (a) Both power transfer and data transfer are in service. (b) Data transfer is in service, and power transfer is on standby. (c) Power transfer is in service, and data transfer is on standby.

the filter output, the OA output, and the output data are shown in oscilloscope channels #1, #2, #3, and #4, respectively. The waveforms in Fig. 8 verify the data transfer principle shown in Fig. 4.

Fig. 9 demonstrates the waveforms for the different operating modes.

1) Both power transfer and data transfer are in service.
2) Data transfer is in service, and power transfer is on standby.
3) Power transfer is in service. And data transfer is on standby.

First, several parameters were concurrently observed in Fig. 9(a). Specifically, the waveforms of the rectified output voltage U_L, the input data, the output waveform from the OA, and the demodulated output data are shown in oscilloscope channels #1, #2, #3, and #4, respectively. In this figure, the data transfer waveform (i.e., channel #3) exhibits minimal interference, ensuring the data can be demodulated effectively. This lack of interference and consequent seamless transfer indicates that the data integrity remains uncompromised by energy fluctuations. Fig. 9(b) illustrates the waveforms observed solely when the data transfer is operational, while the power transfer remains in a standby state. It is observed that these data can be demodulated and transmitted effectively. Notably, there is almost no interference from the data on the energy component as shown in this figure. Similarly, Fig. 9(c) illustrates the waveforms observed

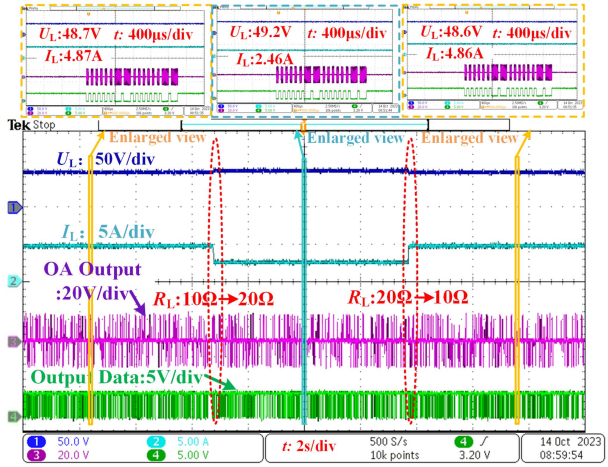

Fig. 10. Dynamic response when the load resistance is changed from 10 to 20 Ω and subsequently reverts to 10 Ω.

solely when the power transfer is operational, while the data transfer remains in a standby state. It also demonstrates that the energy is able to run normally and there is an absence of clutter on the data path, which indicates that the data transfer cannot be interfered with the energy transfer.

In Fig. 10, the dynamic response is presented during a scenario where the load R_L transitions from 10 to 20 Ω and subsequently returns to 10 Ω. This alteration leads to a modification in the output current I_L, sequentially shifting from 4.87 to 2.46 A, and ultimately returning to 4.86 A. Notably, throughout these variations, U_L demonstrates stability, fluctuating marginally from 48.7 to 49.2 V before settling at 48.6 V. Furthermore, it can be seen from the purple (i.e., OA output) and green (i.e., output data) waveforms that data transfer remains stable and can be demodulated normally.

Upon rotating the inner cylinder of the coupler through a full 360° rotation, Fig. 11 shows the waveform alterations corresponding to this dynamic rotation. The zoomed figures showcase data captured at specific rotational angles of 45°, 135°, 225°, and 315°, respectively. It can be observed that the output voltage experiences variations, confined between 47.1 and 48.9 V. In addition, it can be seen from the OA output that there is no detectable significant change in data transfer voltage amplitude, which verifies that data transfer remains relatively stable.

Fig. 12 depicts the experimentally ascertained data pertaining to output voltage and efficiency across a spectrum of angular positions. It indicates that the deviation of the output voltage is ±2.7% of the nominal value of 48 V, evidencing relative stability attributable to consistent mutual inductance. Furthermore, the efficiency metrics observed denote a minimum of 86.7% and a peak of 88.9%. The graphical representation corroborates that both the output voltage and efficiency manifest a commendable degree of constancy throughout the entirety of the angular rotation spanning 0° to 360°.

The measured power loss distribution of the system is presented in Fig. 13. The total power loss under the maximum and minimum efficiency conditions are 27.99 and 35.98 W, respectively.

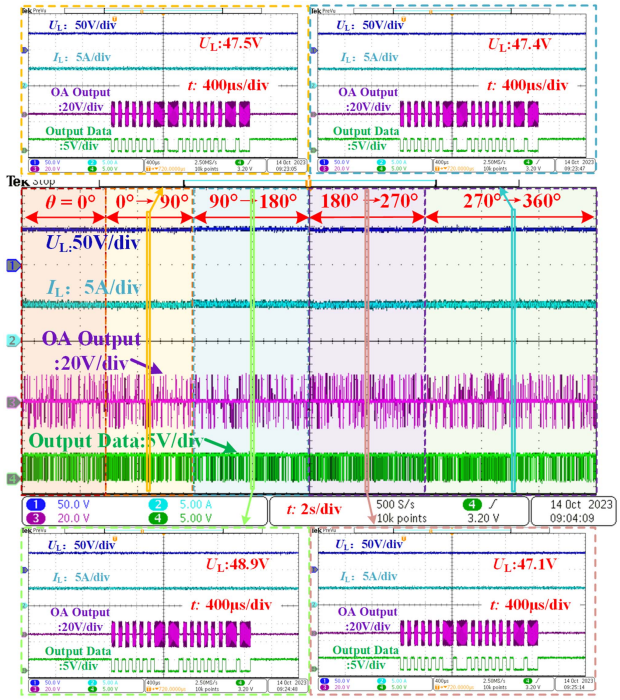

Fig. 11. Variation of the outputs with different angular positions from 0° to 360°.

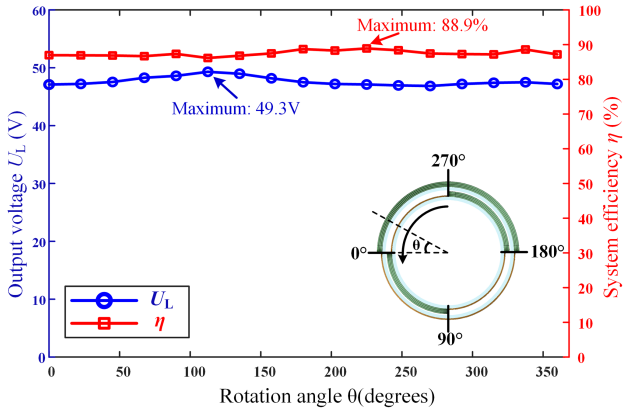

Fig. 12. Experimental validation of the output voltage and efficiency under all 360° rotary conditions.

TABLE III
COMPARISON BETWEEN THIS ARTICLE AND REFERENCES [1], [22], [23], [30]

Ref.	Magnetic coupling structure	Application	Objective
[1]	DD-4D	RSSs	Stable output power during the rotation period
[22]	Four DD and two Q coils	Planar industrial applications	Cross-coupling elimination with double CV outputs
[23]	Two Q and two series-connected perpendicular DD coils	Planar WPT systems	Symmetrical misalignment with data and power transfer
[30]	Two DD and one Q coils	Planar AGV applications	Self-alignment capability and controllable output current
This Paper	Half-cylinder-stator and quarter-cylinder-rotator	RSSs	Both stable data and power transfer capability under 360° rotational conditions

TABLE IV
COMPARISON AMONG DIFFERENT SIMULTANEOUS POWER AND DATA TRANSFER TECHNOLOGIES

Ref.	Type	Feature	Crosstalk	Rotary Application	Method	Characteristic
[4]	Shared channel	Carrier modulation	High	Yes	Adding a series of passive components	Significant interference but suppressed by wave blocking networks
[17]	Shared channel	Energy modulation	High	No	Adjust the input voltage	Forward data transfer; Detecting the output voltage
[18]	Shared channel	Energy modulation	High	No	Adjusting the reflective impedance	Backward data transfer; Detecting the input current
[19]	Shared channel	Carrier modulation	High	No	Adding wave trappers	The added wave trappers need to resonant accurately
[20]	Shared channel	Carrier modulation	High	No	Time-division multiplexing	The difficulty of data demodulation increases with the increase of power level
[21]	Separate channel	Decoupling from distance	Low	No	Separate planar coils	Interference depends on the distance between power and data coupling coils
This work	Separate channel	Decoupling from coil shapes	Low	Yes	Half-cylinder stator and quarter-cylinder-rotator coupling mechanism	DD coils and Q coils are utilized for decoupling; More suitable for volume limited rotary systems

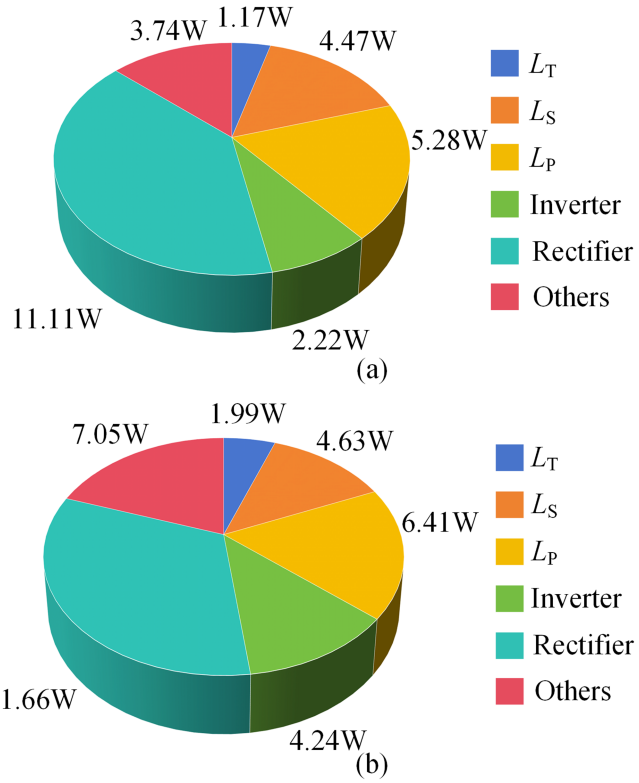

Fig. 13. Measured power loss distribution. (a) Maximum efficiency condition. (b) Minimum efficiency condition.

The measured results of the system signal-to-noise ratio (SNR) with rotation angle are shown in Fig. 14. It can be seen in Fig. 14 that the variation of SNR with rotation angle is relatively small, and data can be demodulated normally at all rotation angles, as the SNR is greater than 0 [19].

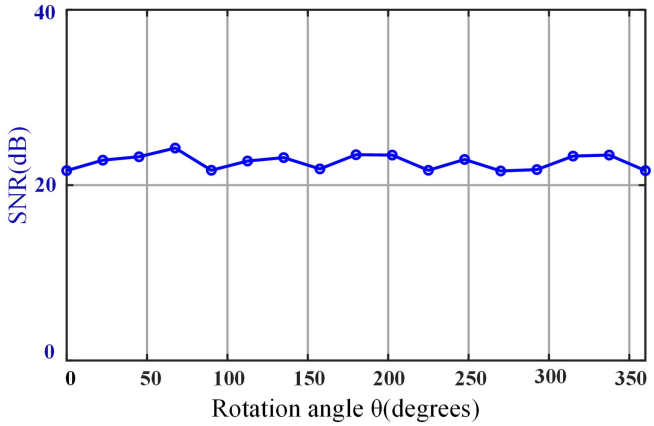

Fig. 14. Measured results of the system SNR with rotation angle.

V. DISCUSSION

A. Novelty of the Presented Magnetic Coupling Structure

Table III presents the comparison results between the proposed method in this article and those proposed in [1], [22], [23], and [30], which highlights the novelty of the presented magnetic coupling structure. First, compared with [22], [23], and [30], the proposed magnetic coupling structure in this article is intended to be applied in rotational applications rather than planar applications. In addition, Ji et al. [1] focus on the stable WPT for the RSSs whereas this system maintains the stability and synchronization of both power and data transfers by using the proposed half-cylinder-stator and quarter-cylinder-rotator magnetic coupling structure.

B. Comparison Results With Other SWPDT Methods

Table IV summarizes a comparison between this article and relevant methods presented in [4], [17], [18], [19], [20], and [21]. First, SWPDT technology can be roughly divided into two types, i.e., shared channel and separate channel.

With respect to the shared channel types [4], [17], [18], [19], [20], the data is integrated into the coupling mechanism for power transfer, thereby facilitating the concurrent transfer of both power and data. Depending on the different methodologies of modulation, this technology can be further categorized into two distinct types: energy modulation [17], [18] and carrier modulation [4], [19], [20]. However, they usually necessitate a

more complex and cost-intensive design of the data processing circuit, largely due to the higher levels of crosstalk interference experienced in their shared channel systems. In contrast, the approach in this study, while requiring extra data transfer coils, simplifies and reduces the cost of circuit design due to the minimal crosstalk between power and data channels.

In the context of separate channel types, the power and data are transmitted via distinct coupling coils in [21]. It indicates that the interference between power and data transfer is comparatively minimal. This interference is attenuated by deliberately augmenting the spatial separation between the power and data coupling mechanisms. However, it necessitates an expanded distance between the power and data channels, leading to an increase in the overall dimensions of the system. Such an enlargement might not be suitable for rotary systems, which are typically constrained by rigorous volume and size limitations. Contrastingly, the work presented in this article avoids such a drawback by achieving decoupling through the use of DD coils and Q coils. As a result, the presented work succeeds in realizing a more compact and efficient structural design, better suited to applications with strict space constraints, such as RSSs.

VI. Conclusion

This article proposes a SWPDT method by utilizing a half-cylinder-stator and quarter-cylinder-rotator coupling mechanism for RSSs. Through this configuration, stability and synchronization of both power and data transfers are ensured, notably under comprehensive 360° rotational conditions. Moreover, based on the decoupling characteristics, the interference between power and data transfer is also greatly reduced. Next, the *LCC*-S topology provides CV output irrespective of load variations, rendering it particularly suitable for RSSs. In addition, the S-S topology for data transfer can effectively improve the reliability of transmission. Experimental results show that in all 0°–360° rotary conditions, the output voltage can be maintained as stable at 48 V with a deviation of $\pm 2.7\%$. The system dc–dc efficiency fluctuates from 86.7% to 88.9%. Furthermore, there is no detectable significant change in data transfer voltage amplitude. In future research, the WPT-based actual RSS will be considered, then the influence of metal skeleton on coupling parameters and the related shielding techniques will be studied.

References

[1] L. Ji, F. Ge, and C. Zhang, "Design of wireless power transmission coupling structure based on rotary steerable drilling," *IEEE Trans. Power Electron.*, early access, doi: 10.1109/TPEL.2023.3319577.

[2] V. Kindl, T. Kavalir, J. Sika, J. Hnatik, M. Krizek, and M. Frivaldsky, "Wireless power transmission system for powering rotating parts of automatic machineries," *Energies*, vol. 15, no. 18, 2022, Art. no. 6856.

[3] A. Abdolkhani, A. P. Hu, and N.-K. C. Nair, "A double stator through-hole type contactless slipring for rotary wireless power transfer applications," *IEEE Trans. Energy Convers.*, vol. 29, no. 2, pp. 426–434, Jun. 2014.

[4] J. Jia, Y. Jia, and X. Li, "Analysis, design, and experimental verification of a parallel wireless power and data transmission method for rotary steering systems," *Energies*, vol. 15, no. 17, 2022, Art. no. 6349.

[5] S. Kisseleff, X. Chen, I. F. Akyildiz, and W. Gerstacker, "Wireless power transfer for access limited wireless underground sensor networks," in *Proc. IEEE Int. Conf. Commun.*, 2016, pp. 1–7.

[6] J. Wei, J. Shiquan, S. Limin, F. Xinsheng, and C. Ping, "Research on rotary navigation drilling tools and its application," *Oil Drilling Prod. Technol.*, vol. 30, no. 5, pp. 21–24, 2008.

[7] L. Ji, M. Zhang, J. Ma, and B. Qian, "A rotary wireless power transfer topology with constant voltage output for oil and gas well," in *Proc. Int. Conf. Power Energy Syst. Appl.*, 2022, pp. 184–190.

[8] X. Li, F. Zheng, H. Wang, Y. Sun, X. Dai, and J. Hu, "A simultaneous power and data transfer method for dynamic wireless charging electric vehicles," *IEEE J. Emerg. Sel. Topics Power Electron.*, vol. 12, no. 1, pp. 328–340, Feb. 2024.

[9] S. Y. R. Hui, Y. Yang, and C. Zhang, "Wireless power transfer: A paradigm shift for the next generation," *IEEE J. Emerg. Sel. Topics Power Electron.*, vol. 11, no. 3, pp. 2412–2427, Jun. 2023.

[10] H. S. Wang, K. W. E. Cheng, and J. F. Hu, "An investigation of compensation networks for three-coil wireless power transfer," in *Proc. 8th Int. Conf. Power Electron. Syst. Appl.*, 2020, pp. 1–6.

[11] J. Liu, F. Xu, C. Sun, and K. H. Loo, "A compact single-phase AC–DC wireless power transfer converter with active power factor correction," *IEEE Trans. Ind. Electron.*, vol. 70, no. 4, pp. 3685–3696, Apr. 2023.

[12] C. Zhang, W. Zou, and N. Cheng, "Overview of rotary steerable system and its control methods," in *Proc. IEEE Int. Conf. Mechatron. Autom.*, 2016, pp. 1559–1565.

[13] M. Uddin and T. Nadeem, "RF-beep: A light ranging scheme for smart devices," in *Proc. IEEE Int. Conf. Pervasive Comput. Commun.*, 2013, pp. 114–122.

[14] H. Liu et al., "Push the limit of WiFi based localization for smartphones," in *Proc. Int. Conf. Mobile Comput. Netw.*, 2012, pp. 305–316.

[15] X. Li, C. Tang, X. Dai, P. Deng, and Y. Su, "An inductive and capacitive combined parallel transmission of power and data for wireless power transfer systems," *IEEE Trans. Power Electron.*, vol. 33, no. 6, pp. 4980–4991, Jun. 2018.

[16] X. He et al., "Wireless power and information dual transfer system via magnetically coupled resonators," *Commun. Eng.*, vol. 3, no. 1, 2024, Art. no. 8.

[17] Y. H. Son and B. J. Jang, "Simultaneous data and power transmission in resonant wireless power system," in *Proc. Asia-Pacific Microw. Conf.*, 2013, pp. 1003–1005.

[18] S. Yue, W. Chen-Chen, T. Chun-Sen, D. Xin, and W. Zhi-Hui, "Study on inductively coupled synchronous transmission of power and signal," *Adv. Technol. Elect. Eng. Energy*, vol. 29, pp. 10–13, 2010.

[19] Y. Sun, P.-X. Yan, Z.-H. Wang, and Y.-Y. Luan, "The parallel transmission of power and data with the shared channel for an inductive power transfer system," *IEEE Trans. Power Electron.*, vol. 31, no. 8, pp. 5495–5502, Aug. 2016.

[20] S. Afshar, S. M. R. Tousi, and H. Karami, "Wireless power and full-duplex data transfer system using the combination of TDM and FDM through a same inductive link," in *Proc. Iranian Conf. Elect. Eng.*, 2018, pp. 1246–1250.

[21] G. Wang, P. Wang, Y. Tang, and W. Liu, "Analysis of dual band power and data telemetry for biomedical implants," *IEEE Trans. Biomed. Circuits Syst.*, vol. 6, no. 3, pp. 208–215, Jun. 2012.

[22] H. Wang and K. W. E. Cheng, "Analysis, design, and validation of a decoupled double-receiver wireless power transfer system with constant voltage outputs for industrial power supplies," *IEEE Trans. Ind. Inform.*, vol. 19, no. 1, pp. 362–370, Jan. 2023.

[23] X. Li, J. Hu, Y. Li, H. Wang, M. Liu, and P. Deng, "A decoupled power and data-parallel transmission method with four-quadrant misalignment tolerance for wireless power transfer systems," *IEEE Trans. Power Electron.*, vol. 34, no. 12, pp. 11531–11535, Dec. 2019.

[24] J. Kim and H. Myung, "Development of a novel hybrid-type rotary steerable system for directional drilling," *IEEE Access*, vol. 5, pp. 24678–24687, 2017.

[25] T. Li et al., "Analysis and design of rotary wireless power transfer system with dual-coupled XLC/S compensation topology," *IEEE Trans. Ind. Appl.*, vol. 59, no. 2, pp. 2639–2649, Mar./Apr. 2023.

[26] Y. Yao, P. Sun, X. Liu, Y. Wang, and D. Xu, "Simultaneous wireless power and data transfer: A comprehensive review," *IEEE Trans. Power Electron.*, vol. 37, no. 3, pp. 3650–3667, Mar. 2022.

[27] Y. Yang, "Precise modeling of nonlinear rectifier loads in wireless power transfer systems," *IEEE J. Emerg. Sel. Topics Power Electron.*, vol. 11, no. 3, pp. 3574–3585, Jun. 2023.

[28] Y. Li, Q. Xu, T. Lin, J. Hu, Z. He, and R. Mai, "Analysis and design of load-independent output current or output voltage of a three-coil wireless power transfer system," *IEEE Trans. Transp. Electrific.*, vol. 4, no. 2, pp. 364–375, Jun. 2018.

[29] J. Liu, F. Xu, C. Sun, and K. H. Loo, "A soft-switched power-factor-corrected single-phase bidirectional AC–DC wireless power transfer converter with an integrated power stage," *IEEE Trans. Power Electron.*, vol. 37, no. 8, pp. 10029–10044, Aug. 2022.
[30] X. Li, C. Wang, H. Wang, X. Dai, Y. Sun, and A. P. Hu, "A robust wireless power transfer system with self-alignment capability and controllable output current for automatic-guided vehicles," *IEEE Trans. Power Electron.*, vol. 38, no. 10, pp. 11898–11906, Oct. 2023.

Xiaofei Li (Member, IEEE) received the B.S. degree in automation and the Ph.D. degree in control theory and control engineering from Chongqing University, Chongqing, China, in 2013 and 2018, respectively.

From 2018 to 2019, he was a Research Associate with the Department of Electrical Engineering, The Hong Kong Polytechnic University. He is currently an Associate Professor with Chongqing University. His research interests include modeling and control of wireless power transfer and power electronics.

Zhiheng Li (Graduate Student Member, IEEE) received the B.E. degree in automation in 2022 from Chongqing University, Chongqing, China, where he is currently working toward the master's degree in control science and engineering.

His main research interests include power electronics and wireless power transfer.

Udaya K. Madawala (Fellow, IEEE) received the B.Sc. (Hons.) degree in electrical engineering from the University of Moratuwa, Moratuwa, Sri Lanka, in1986, and the Ph.D. degree in power electronics from the University of Auckland, Auckland, New Zealand, in 1993, as a Commonwealth Doctoral Scholar.

He is currently a Full Professor. He has more than 250 IEEE and IET journal and international conference publications and holds a number of patents related to wireless power transfer and power converters. He has more than 30 years of both industry and research experience in the fields of power electronics and energy. His research interests include power electronics, wireless power transfer, vehicle-to-grid applications, and renewable energy.

Dr. Madawala is a Distinguished Lecturer of IEEE Power Electronic Society. He has served both IEEE Power Electronics and Industrial Electronics Societies in numerous roles, relating to conferences, technical committees, and chapter activities. He is currently an Associate Editor of IEEE TRANSACTIONS ON POWER ELECTRONICS, and a member of the Sustainable Energy Systems Technical Committee and the Oceania Liaison Chair of Membership Development Committee of IEEE Power Electronics Society.

Heshou Wang received the M.Sc. and Ph.D. degrees in electrical engineering from The Hong Kong Polytechnic University, Hong Kong, in 2018 and 2022, respectively.

From 2018 to 2019, he was a Research Assistant with the Department of Electrical Engineering, The Hong Kong Polytechnic University, where he is currently a Postdoctoral Fellow. His main research interests include applied electromagnetics, wireless power transfer, and electric vehicles.

Yue Sun (Member, IEEE) received the B.E. degree in electrical engineering, the M.E. degree in industrial automation, and the Ph.D. degree in mechanical electrical integrated manufacturing from Chongqing University, Chongqing, China, in 1982, 1988, and 1995, respectively.

In 1997, he was a Senior Visiting Scholar with the University of Valenciennes, Valenciennes, France. He is currently a Professor with the School of Automation, Chongqing University. His current research interests include automatic control, wireless power transfer, and power electronics applications.

Xin Dai (Member, IEEE) received the B.E. degree in industrial automation from Yuzhou University, Chongqing, China, in 2000, and the Ph.D. degree in control theory and control engineering from the College of Automation, Chongqing University, Chongqing, China, in 2006.

In 2012, he was a Visiting Scholar with The University of Auckland, Auckland, New Zealand. He is currently a Professor with the College of Automation, Chongqing University. His current research interests include inductive power transfer technology and nonlinear dynamic behavior analysis of power electronics.

Jiefeng Hu (Senior Member, IEEE) received the Ph.D. degree in electrical engineering from University of Technology Sydney, Ultimo, Australia, in 2013.

He participated in the research of minigrids with Commonwealth Scientific and Industrial Research Organization, Newcastle, Australia. He was an Assistant Professor with The Hong Kong Polytechnic University, Kowloon, Hong Kong. He is currently an Associate Professor and a Program Coordinator of Electrical Engineering with Federation University Australia, Ballarat, VIC, Australia, where he is also a Stream Leader of Centre for New Energy Transition Research. His research interests include power electronics, renewable energy, and smart microgrids.

Dr. Hu is an Associate Editor for *IET Renewable Power Generation*, an Editor for IEEE TRANSACTIONS ON ENERGY CONVERSION, an Associate Editor for IEEE ACCESS, and was a Guest Editor for IEEE TRANSACTIONS ON INDUSTRIAL ELECTRONICS for a Special Issue "Applications of Predictive Control in Microgrids."